The Journal of Chemical Physics

Low-frequency excitation of singlet–triplet transitions. Application to nuclear hyperpolarization

Cite as: J. Chem. Phys. **155**, 154201 (2021); https://doi.org/10.1063/5.0065863
Submitted: 05 August 2021 • Accepted: 31 August 2021 • Published Online: 15 October 2021

Laurynas Dagys, Christian Bengs and Malcolm H. Levitt

COLLECTIONS

This paper was selected as Featured

View Online Export Citation CrossMark

ARTICLES YOU MAY BE INTERESTED IN

Solving the Schrödinger equation using program synthesis
The Journal of Chemical Physics **155**, 154102 (2021); https://doi.org/10.1063/5.0062497

What the foundations of quantum computer science teach us about chemistry
The Journal of Chemical Physics **155**, 150901 (2021); https://doi.org/10.1063/5.0060367

Nuclear singlet relaxation by chemical exchange
The Journal of Chemical Physics **155**, 124311 (2021); https://doi.org/10.1063/5.0066182

Lock-in Amplifiers up to 600 MHz
Zurich Instruments
Watch

© 2021 Author(s).

The Journal of Chemical Physics ARTICLE scitation.org/journal/jcp

Low-frequency excitation of singlet–triplet transitions. Application to nuclear hyperpolarization

Cite as: J. Chem. Phys. 155, 154201 (2021); doi: 10.1063/5.0065863
Submitted: 5 August 2021 • Accepted: 31 August 2021 •
Published Online: 15 October 2021

View Online Export Citation CrossMark

Laurynas Dagys, Christian Bengs, and Malcolm H. Levitt[a)]

AFFILIATIONS

Department of Chemistry, University of Southampton, Southampton SO17 1BJ, United Kingdom

[a)]Author to whom correspondence should be addressed: mhl@soton.ac.uk

ABSTRACT

Coupled pairs of nuclear spin-1/2 support one singlet state and three triplet states. Transitions between the singlet state and one of the triplet states may be driven by an oscillating low-frequency magnetic field, in the presence of couplings to a third nuclear spin, and a weak bias magnetic field. The oscillating field is in the same direction as the bias field and is called a WOLF (Weak Oscillating Low Field) pulse. Application of a WOLF pulse allows for the generation of strong nuclear hyperpolarization of ^{13}C nuclei, starting from the nuclear singlet polarization of a ^{1}H spin pair, associated with the enriched *para*-spin isomer of hydrogen gas. Hyperpolarization is demonstrated for two molecular systems.

© 2021 Author(s). All article content, except where otherwise noted, is licensed under a Creative Commons Attribution (CC BY) license (http://creativecommons.org/licenses/by/4.0/). https://doi.org/10.1063/5.0065863

I. INTRODUCTION

Magnetic resonance experiments usually involve the application of a strong magnetic field (typically from a fraction of one Tesla to up to tens of Tesla) combined with radio frequency pulses (for nuclear magnetic resonance, NMR) or microwave pulses (for electron spin resonance, ESR) that are resonant with the magnetic Zeeman transitions of the system. In these high-field conditions, the parts of the spin Hamiltonian that do not commute with the Zeeman Hamiltonian are usually removed. This *secular approximation* leads to a major simplification of spin dynamical theory and is one of the cornerstones of the modern NMR theory.[1] One consequence is that all transitions involving combinations or multiples of the Larmor frequencies are not observed in NMR or ESR spectra. Some exceptions to this paradigm exist, such as "overtone" transitions in the NMR of nuclei with large quadrupolar moments[2] and the use of non-secular hyperfine couplings in solid-effect dynamic nuclear polarization[3] and stimulated nuclear polarization.[4]

In the case of NMR, the secular approximation breaks down into very small magnetic fields such that the Larmor frequencies are comparable in magnitude to the spin–spin interactions.[5] Here, we show that the mixing of states by non-secular spin–spin couplings in the low-field regime allows selected "forbidden" transitions to be induced by oscillating magnetic fields. In suitable circumstances, this phenomenon allows for the generation of strong hyperpolarization in the reaction products of hydrogen gas enriched in the *para*-spin isomer. We demonstrate the generation of two small molecules in solution with high levels of ^{13}C polarization. One of these substances, fumarate, is a natural metabolite, which has been used for the characterization of cancer in magnetic resonance imaging (MRI).[6]

II. THEORY

Consider an ensemble of nuclear three-spin-1/2 systems, each consisting of two nuclei I_1 and I_2 of one isotopic type with magnetogyric ratio γ_I and a third nucleus S_3 of a different isotopic type with magnetogyric ratio γ_S. In the isotropic solution state, the three nuclei mutually interact by scalar spin–spin coupling terms, mediated by the bonding electrons. These couplings consist of a homonuclear coupling J_{12} and two heteronuclear couplings J_{13} and J_{23}. The two heteronuclear couplings are assumed to be different, $J_{13} \neq J_{23}$. In the absence of any external fields, the Hamiltonian of such a configuration is given by

© Author(s) 2021

$$H_J = 2\pi J_{12}\boldsymbol{I}_1\cdot\boldsymbol{I}_2 + 2\pi J_{13}\boldsymbol{I}_1\cdot\boldsymbol{I}_3 + 2\pi J_{23}\boldsymbol{I}_2\cdot\boldsymbol{I}_3. \quad (1)$$

The presence of external magnetic fields is incorporated by coupling the individual spin angular momenta to the external magnetic field, taking their respective gyromagnetic ratios into account. For an I_2S-spin system, the magnetic Hamiltonian is given as follows:

$$H_M(t) = -\gamma_I\mathbf{B}(t)\cdot(\boldsymbol{I}_1+\boldsymbol{I}_2) - \gamma_S\mathbf{B}(t)\cdot\boldsymbol{I}_3, \quad (2)$$

so that the total spin Hamiltonian is given by

$$H(t) = H_J + H_M(t). \quad (3)$$

A. WOLF pulses

Consider now the application of a small magnetic field B_z along the laboratory frame z axis. For a WOLF pulse, we may represent this field as the sum of a time-independent "bias" field B_{bias} and a time-dependent oscillating field, denoted as B_{WOLF},

$$B_z(t) = B_{\text{bias}} + B_{\text{WOLF}}(t). \quad (4)$$

The oscillating field is explicitly given by

$$B_{\text{WOLF}}(t) = B^0_{\text{WOLF}}\cos(\omega_{\text{WOLF}}t), \quad (5)$$

where ω_{WOLF} is the frequency of the oscillating field and B^0_{WOLF} is its peak amplitude. Since the applied oscillating field is small in magnitude and low in frequency, we refer to the oscillating magnetic field as a WOLF (*Weak Oscillating Low Frequency*) pulse.

Note that the B_{bias} and B_{WOLF} fields are applied in the *same direction*. This geometry differs from most NMR experiments, where oscillating fields are applied transverse to the main field, with few exceptions.[2,7,8] The Hamiltonian describing the interaction with the externally applied fields therefore reduces to

$$H_M(t) = -\gamma_I B_z(t)(I_{1z}+I_{2z}) - \gamma_S B_z(t)S_z. \quad (6)$$

If the magnetic fields are low enough that chemical shifts are negligible, the spin Hamiltonian may be decomposed as a sum of five terms as follows:

$$\begin{aligned} H(t) &= H_J + H_M(t) \\ &= H_A + H_B + H_C + H_D + H_{\text{WOLF}}(t). \end{aligned} \quad (7)$$

The individual contributions are given by

$$\begin{aligned} H_A &= -B_{\text{bias}}(\gamma_I(I_{1z}+I_{2z}) + \gamma_S S_{3z}) \\ &\quad + 2\pi J_{12}\boldsymbol{I}_1\cdot\boldsymbol{I}_2 + \pi(J_{13}+J_{23})(I_{1z}+I_{2z})S_{3z}, \\ H_B &= \pi(J_{13}-J_{23})(I_{1z}-I_{2z})S_{3z}, \\ H_C &= \frac{1}{2}\pi(J_{13}+J_{23})\times(I_1^+S_3^- + I_2^+S_3^- + I_1^-S_3^+ + I_2^-S_3^+), \\ H_D &= \frac{1}{2}\pi(J_{13}-J_{23})(I_1^+S_3^- - I_2^+S_3^- + I_1^-S_3^+ - I_2^-S_3^+), \\ H_{\text{WOLF}}(t) &= -B_{\text{WOLF}}(t)(\gamma_I(I_{1z}+I_{2z}) + \gamma_S S_{3z}). \end{aligned} \quad (8)$$

The terms H_A, H_C, and H_{WOLF} are symmetric with respect to the exchange of the two I-spins, while the terms H_B and H_D are antisymmetric. If the Larmor frequency of the nuclei in the bias field is larger than that of the spin–spin couplings and the difference between the heteronuclear couplings is smaller than that in the homonuclear couplings ($|J_{13}-J_{23}| \ll |J_{12}|$, i.e., near-equivalence[9]), then the H_A term dominates. The terms H_C and H_{WOLF} commute with H_A and may be regarded as secular, while the terms H_B and H_D do not commute with H_A and are non-secular. The terms H_B and H_C both give rise to small eigenvalue shifts, which are neglected here for the sake of brevity. The exchange-antisymmetric non-secular term H_D is the most important one for the purposes of this paper. The eigenstates and eigenvalues of H_A are sketched in Fig. 1. The eigenstates are direct products of the singlet and triplet states of the I-spin pair with the Zeeman states of the S-spin such that the triplet product states are symmetric and the singlet product states are anti-symmetric under permutation of spins 1 and 2,

$$\begin{aligned} (12)|T_M m_S\rangle &= (+1)|T_M m_S\rangle, \\ (12)|S_0 m_S\rangle &= (-1)|S_0 m_S\rangle, \end{aligned} \quad (9)$$

where $M \in \{-1, 0, 1\}$ and the Zeeman eigenequations are

$$\begin{aligned} (I_{1z}+I_{2z})|T_M m_S\rangle &= M|T_M m_S\rangle, \\ (I_{1z}+I_{2z})|S_0 m_S\rangle &= 0, \\ S_{3z}|T_M m_S\rangle &= m_S|T_M m_S\rangle, \\ S_{3z}|S_0 m_S\rangle &= m_S|S_0 m_S\rangle. \end{aligned} \quad (10)$$

The symbols α and β are used to denote $m_S = \pm\frac{1}{2}$, respectively. The symbol (12) indicates the permutation of the two ^{1}H spins.

Consider the transition between the $|S_0\beta\rangle$ and $|T_{-1}\alpha\rangle$ states, indicated in Fig. 1. This transition is "forbidden" since all off-diagonal matrix elements of the form $\langle S_0\beta|(I_{1\mu}+I_{2\mu})|T_{-1}\alpha\rangle$ are zero for $\mu \in \{x, y, z\}$. In fact, all Hamiltonian terms in Eq. (8) have a

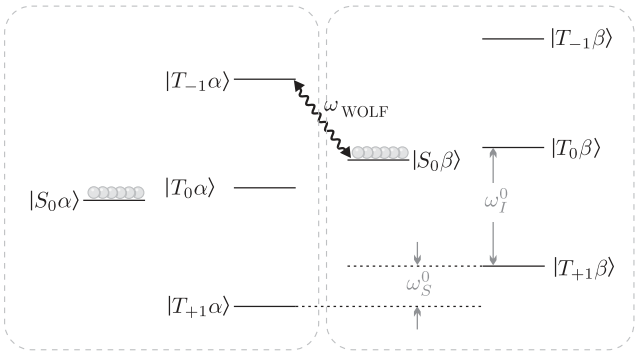

FIG. 1. Eigenvalues and eigenstates of H_A [Eq. (8)] for a system of two I-spins and one S-spin in the near-equivalence limit ($|J_{13}-J_{23}| \ll |J_{12}|$). The circles represent the population distribution for a fully populated singlet state between the two I-spins. The Larmor frequencies in the bias field B_{bias} are indicated: $\omega_I^0 = -\gamma_I B_{\text{bias}}$ for the I-spins and $\omega_S^0 = -\gamma_S B_{\text{bias}}$ for the S-spins. The WOLF pulse is applied with a frequency ω_{WOLF} matching the transition frequency ω_{ST} between the indicated pair of states [Eq. (12)].

© Author(s) 2021

zero matrix element connecting these two states, except for the non-secular antisymmetric term H_D, with matrix elements given by

$$\langle S_0\beta|H_D|T_{-1}\alpha\rangle = \langle T_{-1}\alpha|H_D|S_0\beta\rangle = 2^{-1/2}\pi(J_{13} - J_{23}). \tag{11}$$

The difference between the corresponding diagonal elements of H_A is given by

$$\begin{aligned}\omega_{ST} &= \langle T_{-1}\alpha|H_A|T_{-1}\alpha\rangle - \langle S_0\beta|H_A|S_0\beta\rangle \\ &= B_{\text{bias}}(\gamma_I - \gamma_S) + \frac{\pi}{2}(4J_{12} - J_{13} - J_{23}),\end{aligned} \tag{12}$$

where the notation ω_{ST} indicates "singlet–triplet transition." Note that this transition frequency includes a combination of I-spin and S-spin Larmor frequencies.

The term H_D induces a slight mixing of these two H_A eigenstates. The small degree of state mixing would have very little effect if it were not for the time-dependence introduced by the coupling to the oscillating magnetic field, $H_{\text{WOLF}}(t)$. If the oscillation frequency matches the singlet–triplet transition frequency ($|\omega_{\text{WOLF}}| \simeq |\omega_{ST}|$), the periodic time-dependence drives coherent transitions between these two eigenstates. For example, suppose that the initial state of the system consists of a strongly populated state $|S_0\beta\rangle$ and a completely depleted state $|T_{-1}\alpha\rangle$. The density operator is described by

$$\begin{aligned}\langle S_0\beta|\,\rho(0)\,|S_0\beta\rangle &= 1, \\ \langle T_{-1}\alpha|\,\rho(0)\,|T_{-1}\alpha\rangle &= 0.\end{aligned} \tag{13}$$

Consider a WOLF pulse applied for a duration τ on the resonance condition $\omega_{\text{WOLF}} = \omega_{ST}$. As discussed in more detail in the Appendix, the spin-state populations after the pulse are approximately given by

$$\begin{aligned}\langle S_0\beta|\,\rho(\tau)\,|S_0\beta\rangle &\simeq \frac{1}{2}\Big(1 + \cos(\omega_{\text{nut}}^{ST}\tau)\Big), \\ \langle T_{-1}\alpha|\,\rho(\tau)\,|T_{-1}\alpha\rangle &\simeq \frac{1}{2}\Big(1 - \cos(\omega_{\text{nut}}^{ST}\tau)\Big),\end{aligned} \tag{14}$$

where the singlet–triplet nutation frequency under the WOLF pulse is given by

$$\omega_{\text{nut}}^{ST} = 2\pi\sqrt{J_{13}^2 + J_{23}^2}\,\sin(\phi + \theta/2)J_1(A). \tag{15}$$

The angles θ and ϕ are given by

$$\begin{aligned}\theta &= \arctan2(2J_{12}, J_{13} - J_{23}), \\ \phi &= \arctan2(J_{13} + J_{23}, J_{13} - J_{23})\end{aligned} \tag{16}$$

such that $\theta, \phi \ll 1$ in the near-equivalence regime.

The symbol J_1 denotes a Bessel function of the first kind with its argument given by

$$A = (\gamma_I - \gamma_S)B_{\text{WOLF}}^0/\omega_{ST}. \tag{17}$$

These equations apply approximately in the limits $|J_{13} - J_{23}| \ll |J_{12}|$ and $J_{13}^2 + J_{23}^2 \ll \omega_{ST}^2$.

It is therefore possible to transport population completely from one state to the other by applying a WOLF pulse of duration $\pi/\omega_{\text{nut}}^{ST}$. The inversion speed is maximized by choosing the peak amplitude of the WOLF pulse to equal $B_{\text{WOLF}}^0 \simeq 2B_{\text{bias}}$ at which point the Bessel function $J_1(A)$ reaches its approximate maximum. Since there are practical limits on the generation of large oscillating magnetic fields, this technique is most appropriate for low-field magnetic resonance.

Note that an oscillating *transverse* field at the frequency ω_{WOLF} has a negligible effect since all matrix elements of the form $\langle\phi|I_{1x} + I_{2x}|\phi'\rangle$ are equal to zero, where $|\phi\rangle$ and $|\phi'\rangle$ are either $|S_0\beta\rangle$ or $|T_{-1}\alpha\rangle$.

The use of oscillating magnetic fields for the selective excitation of transitions has previously been explored in the context of ultralow-field NMR.[8] However, those experiments follow the familiar paradigm of resonant excitation in which transitions are induced by modulating off-diagonal Hamiltonian terms at a frequency that matches the transition energy. In the current case, on the other hand, the off-diagonal non-secular terms are time-independent, and it is the diagonal terms that are given a periodic time-dependence by the oscillating applied field. There is a distant relationship with selective excitation in magic-angle-spinning solid-state NMR.[10]

B. Parahydrogen-induced polarization

The resonant driving of singlet–triplet transitions is particularly useful in the context of parahydrogen-induced polarization (PHIP), a technique which is widely used to enhance NMR signals.[11–29] In this method, hydrogen gas is enriched in the *para*-spin isomer and reacted with a substrate in the presence of a catalyst. The proton pair of the product molecule exhibits excess population in the singlet state. The strongly enhanced singlet spin order is converted into hyperpolarized magnetization of heteronuclei such as ^{13}C by applying a sequence of magnetic fields. A range of suitable techniques has been developed.[15–23,26,30,31]

We now show that the application of a WOLF pulse in a small bias magnetic field leads to strong hyperpolarization of ^{13}C nuclei in the reaction products of *para*-enriched H_2 gas, with potential advantages over other methods, as discussed below.

The principle of the experiment is shown in Fig. 1. The spin-state populations (indicated by balls) are given for the case that the spins I_1 and I_2 are protons originating from the *para*-enriched hydrogen and the spin S_3 is a ^{13}C nucleus in the product molecule. The populations of the $|S_0\alpha\rangle$ and $|S_0\beta\rangle$ states are strongly enhanced due to their provenance as the nuclei of the *para*-enriched H_2 spin isomer. Since these two populations are equal, there is no polarization of the S-spin at this stage. However, if the WOLF pulse transports the population from the $|S_0\beta\rangle$ state to the $|T_-\alpha\rangle$ state, as shown in Eq. (14), the resulting population distribution has excess population in the $|S_0\alpha\rangle$ and $|T_-\alpha\rangle$ states. Since the S-spin is in the state $|\alpha\rangle$ in both cases, this corresponds to a high degree of ^{13}C polarization. A ^{13}C polarization of the order of unity represents an enhancement of the ^{13}C NMR signals by around five orders of magnitude, relative to ordinary NMR based on thermal equilibrium polarization in a strong magnetic field.

We propose the acronym WEREWOLF (Whopping Enhancement Realized by Excitation With Oscillating Low Field) for *para*-hydrogen-induced polarization of heteronuclei using WOLF pulses for the singlet–triplet population transfer.

© Author(s) 2021

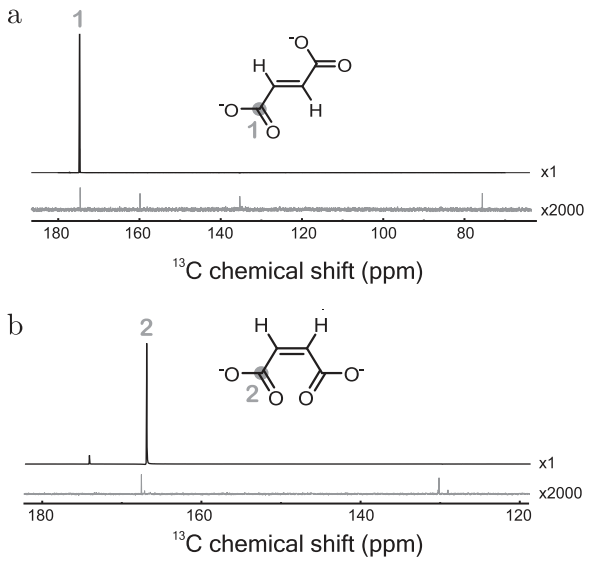

FIG. 2. ^{1}H-decoupled ^{13}C spectra of (a) fumarate and (b) maleate at a field of 9.41 T. Single-transient WEREWOLF-hyperpolarized ^{13}C spectra are compared with conventional ^{13}C NMR spectra acquired at thermal equilibrium, averaged over 360 transients (for fumarate) or 512 transients (for maleate). The strong ^{13}C peaks are from hyperpolarized naturally occurring ^{13}C nuclei at the molecular sites, indicated by filled circles. The ^{13}C peaks at 160 and 76 ppm in (a) correspond to unreacted disodium acetylene dicarboxylate. The small signal at 172 ppm in (b) is attributed to succinate generated by secondary hydrogenation. The change in the chemical shift for the maleate ^{13}C peak in (b) is provisionally attributed to a change in sample temperature.

III. METHODS

A. Materials

The substances fumarate (*E*-butenedioate) and maleate (*Z*-butenedioate) were used for demonstrations of WEREWOLF. The chemical structures are shown in Fig. 2. The precursor solution for fumarate was prepared by dissolving 100 mM disodium acetylene dicarboxylate, 100 mM sodium sulfite, and 6 mM $[RuCp^{*}(MeCN)_3]PF_6$ (CAS number: 99 604-67-8) in D_2O, heating to 60 °C, and passing through a Millex® 0.22 μm PES filter.

The precursor solution for maleate was prepared by dissolving 100 mM acetylene dicarboxylic acid and 5 mM $[Rh(dppb)(COD)]BF_4$ (CAS number: 7440-16-6) in methanol-d_4. All materials and consumables were purchased from Merck.

Para-enriched hydrogen was produced by passing hydrogen gas over an iron oxide catalyst packed in a 1/4 in. stainless steel tube and cooled with liquid nitrogen.

Under the reaction and solvent conditions used for the experiments, maleate is expected to exist mainly in the form of the protonated singly charged mono-hydrogen maleate anion, while fumarate is expected to exist as the doubly charged non-protonated fumarate anion. These protonation states are ignored in the current report for the sake of simplicity.

About 2% of fumarate and maleate molecules contain a naturally occurring ^{13}C nucleus at the sites shown in Fig. 2. The two ^{1}H nuclei and the ^{13}C nucleus form a three-spin-1/2 system of the type discussed above. The *J*-coupling parameters for the two molecular systems are given in Table I.

TABLE I. Spin–spin coupling parameters for (1-^{13}C)fumarate and (1-^{13}C)maleate, adapted from Ref. 19.

Compound	J_{12} (Hz)	J_{23} (Hz)	J_{13} (Hz)
Fumarate	15.9	5.8	3.3
Maleate	12.3	12.9	2.5

B. Equipment

A sketch of the equipment is shown in Fig. 3. The hydrogen gas is bubbled through the solutions using a 1/16 in. PEEK capillary tube inserted inside a thin-walled Norell® pressure NMR tube. The Rheodyne MXP injection valves and the Keysight 33500B

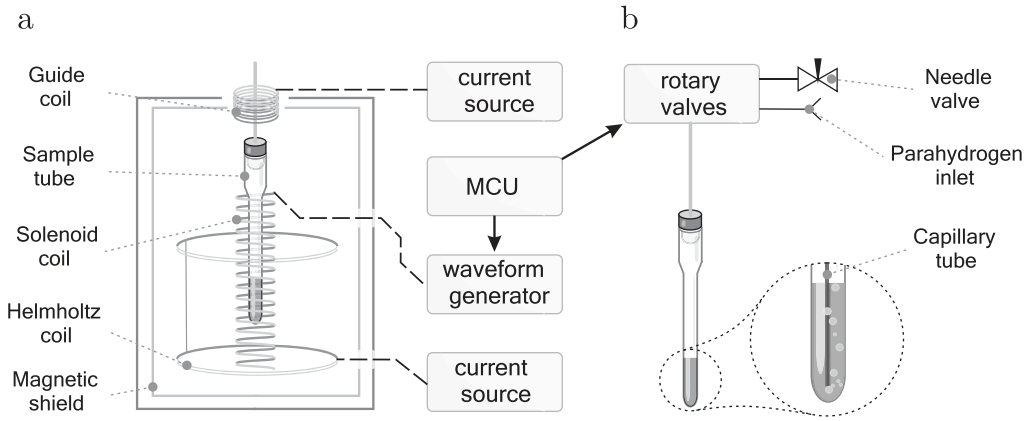

FIG. 3. Schematic diagram of the experimental setup. (a) Mu-metal shield and associated components. During the WOLF pulse, the Helmholtz coil generates the bias field B_{bias}, whereas the solenoid coil produces the oscillating field $B_{WOLF}(t)$. (b) Gas-handling apparatus, including a thick-wall NMR tube equipped with a capillary for the *para*-enriched H_2 gas. MCU—micro-controller unit.

© Author(s) 2021

waveform generator were triggered and controlled using an Arduino Mega 2560 micro-controller board. The waveform generator was connected to the 3 cm wide and 30 cm long solenoid coil of 300 turns placed in a TwinLeaf MS-4 mu-metal shield and used for generating the oscillating magnetic field. The bias field was generated by using the built-in Helmholtz coil of the Twinleaf shield, powered by a Keithley 6200 DC current source. An ~200 turn solenoid guide coil was wound around the orifice penetrating the mu-metal shield and continuously driven by a second Keithley 6200 DC current source to produce the 6 μT field. The guide coil was used to avoid zero-field crossings during sample transportation.[10]

C. Experimental procedure

Figure 4 shows a timing diagram of the WEREWOLF experiment, showing the magnetic fields experienced by the sample as a function of time. Each experiment starts by warming 250 μl of the sample mixture to ~90 °C in the ambient magnetic field of the laboratory (~110 μT), followed by insertion into the magnetic shield. *Para*-enriched hydrogen gas is bubbled through the solution at 6 bar pressure. The bubbling time τ_b was set to 30 and 10 s for experiments involving fumarate and maleate, respectively. The oscillating WOLF pulse is applied for an interval τ in the presence of a bias field of B_{bias} = 2 μT. For the experiments shown here, the WOLF pulse was arbitrarily set to B^0_{WOLF} = 2 μT, which is one-half of its optimal value according to theory. At the end of the WOLF pulse, the bias field is increased for a few seconds and the sample was manually removed from the shield and inserted by hand into the 9.41 T NMR magnet.

The ^{13}C free-induction decays were excited by a hard pulse of 14.7 kHz rf amplitude and recorded with 65 K point density at the spectral width of 200 ppm using a Bruker Avance Neo spectrometer. Additional ^{1}H decoupling was used for all experiments. Thermal equilibrium ^{13}C spectra were recorded at room temperature with recycle delays of 120 s, averaging the signals from 512 to 360 transients for maleate and sodium fumarate, respectively.

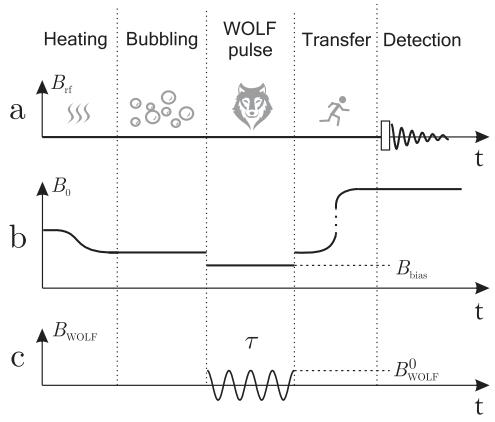

FIG. 4. Timing diagram for the WEREWOLF procedure, involving bubbling of the sample with *para*-enriched hydrogen gas and a sequence of magnetic fields. (a) ^{13}C radio frequency pulse applied in a high magnetic field at the end of the procedure and NMR signal acquisition. (b) Magnetic field along the *z* axis, showing the ambient laboratory field during sample heating, the reduction in the field as the sample is placed in the shield, the bias field B_{bias} during the WOLF pulse, the removal of the sample from the shield, and insertion into the high-field NMR magnet. (c) Oscillating WOLF pulse field, applied for a duration τ, with a frequency ω_{WOLF} and peak amplitude B^0_{WOLF}. The total field experienced by the sample is the sum of (b) and (c).

IV. RESULTS

Figure 2 shows single-transient hyperpolarized ^{13}C NMR spectra for (a) fumarate and (b) maleate, obtained using the WEREWOLF procedure. The WOLF pulse parameters were $\omega_{WOLF}/2\pi$ = 77.3 Hz and τ = 0.65 s for fumarate and $\omega_{WOLF}/2\pi$ = 74.0 Hz and τ = 0.12 s for maleate.

Conventional ^{13}C NMR spectra obtained by multiple signal acquisitions on the hydrogenated samples after thermal equilibration are also shown in Fig. 2. A comparison of these spectra allows for the estimation of the ^{13}C polarization levels achieved by WEREWOLF, which are $p \simeq 8\%$ for fumarate and $p \simeq 19\%$ for maleate. These results are highly competitive with previous work,[28,31,33,34] especially when the relatively low *para*-hydrogen enrichment levels, crude apparatus, manual sample transport, and sub-optimal reaction conditions are taken into account.

Integrated ^{13}C signal amplitudes as a function of the WOLF pulse duration τ are shown in Fig. 5. The coherent oscillations of the hyperpolarized magnetization are striking. Each experimental point was obtained from a separate experiment on a fresh sample. The normalized experimental data are compared with numerical simulations and analytical curves derived from Eqs. (14) and

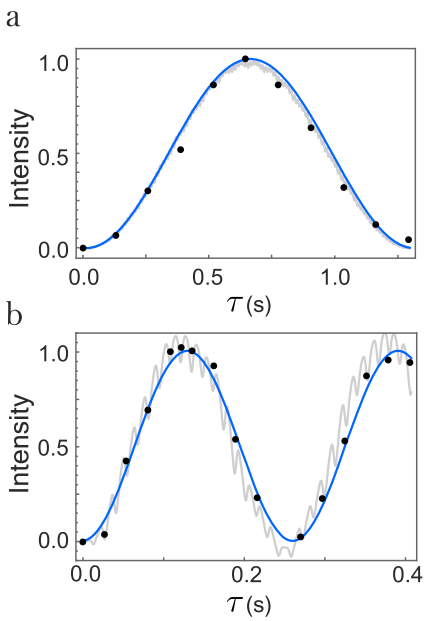

FIG. 5. Hyperpolarized fumarate (a) and maleate (b) ^{13}C signal intensities as a function of the WOLF pulse duration τ. The WOLF pulse frequencies are 77.3 Hz for fumarate and 74.0 Hz for maleate. The black dots depict integrated experimental signal amplitudes, normalized to 1 for the maximum value. The gray lines represent numerical *SpinDynamica*[32] simulations for the coupling parameters in Table I. The blue lines show analytical solutions given by Eq. (14). All values of τ used for the experiments are integer numbers of the WOLF period $2\pi/\omega_{WOLF}$, which are 12.94 ms for fumarate and 13.51 ms for maleate.

© Author(s) 2021

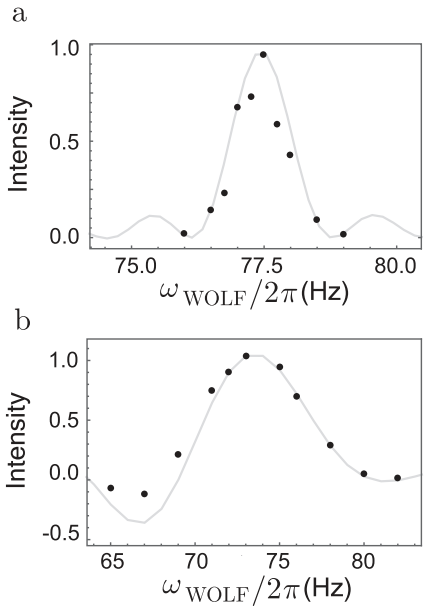

FIG. 6. Hyperpolarized fumarate (a) and maleate (b) ^{13}C signal intensity as a function of WOLF pulse frequency ω_{WOLF}. The pulse duration τ is set to 0.65 s for fumarate and 0.12 s for maleate. The black dots depict integrated experimental signal amplitudes, normalized to 1 for the maximum value. The gray lines represent numerical *SpinDynamica*[32] simulations for the coupling parameters in Table I.

(15). The agreement between both curves and the experimental data is gratifying. The oscillations are much faster for maleate than for fumarate, mainly because the difference in heteronuclear J-couplings is 10.4 Hz for maleate but only 2.5 Hz for fumarate (see Table I).

As discussed in Sec. II A, the singlet–triplet transition is effectively driven once the condition $\omega_{WOLF} = \omega_{ST}$ is fulfilled. This is evident in Fig. 6, which displays hyperpolarized ^{13}C signal intensity as a function of ω_{WOLF} at fixed WOLF pulse duration. The experimental data points indicate a sharp resonance for fumarate with a full-width-at-half-maximum (FWHM) of ~ 0.4 Hz, whereas a larger FWHM of ~ 6 Hz is observed for maleate. The experimental frequency profiles match well the numerical simulations, indicated by solid lines. The good agreement indicates that the effects of field inhomogeneity were minor in this case.

V. CONCLUSIONS

Magnetic resonance phenomena involving non-secular spin–spin couplings are normally encountered in systems with large nuclear quadrupolar couplings[2] or hyperfine couplings to unpaired electrons, as in solid-effect dynamic nuclear polarization (DNP)[3] and stimulated nuclear polarization in photochemical reactions involving transient radical pairs.[4] The work described here shows that non-secular out-of-pair couplings may also be exploited in purely nuclear spin systems, albeit at an energy scale, which is ~ 9 orders of magnitude lower than in solid-effect DNP. Here, too, non-secular effects allow "forbidden" transitions to couple to the electromagnetic field, allowing for the generation of strong nuclear hyperpolarization.

Many other methods have been described for the transformation of ^{1}H singlet order to ^{13}C magnetization, including pulse techniques,[15–19] field-cycling and level-anticrossing phenomena,[20–23] and low-field methods.[22–25,29,30] However, most of these schemes are active in either the "ultralow-field" regime (Larmor frequencies less than or comparable to J-couplings) or the "high-field" regime of conventional NMR spectroscopy. Both of these regimes are associated with some disadvantages: The ultralow-field regime is associated with short coherence lifetimes through couplings to quadrupolar nuclear isotopes,[27] such as ^{2}H and ^{14}N, while the high-field regime of conventional NMR is associated with the singlet–triplet conversion of the dissolved *para*-hydrogen gas, leading to reduced polarization levels of the product molecules.[33,35,36]

The WOLF method described here provides a fast exchange of singlet and triplet populations. The bias field is conveniently applied in the same direction as the WOLF pulse and may, in principle, be set to any value within technical constraints. A small bias field of a few μT is sufficient to resolve the Larmor frequencies of the different nuclear isotopes. In principle, this should make it possible to implement heteronuclear spin decoupling by resonant transverse oscillating fields. Furthermore, the coherent nature of the singlet–triplet conversion should allow for deployment of the full palette of "pulse tricks" developed for conventional high-field NMR, including error-compensating composite pulses.[37] Applications are envisaged to other hyperpolarization techniques, such as the SABRE (Signal Amplification by Reversible Exchange) method.[13,26] The method described here might be related to some recent variants of SABRE, which also use periodically modulated magnetic fields.[24,29]

ACKNOWLEDGMENTS

We acknowledge funding received from the Marie Skłodowska-Curie program of the European Union (Grant No. 766402), the European Research Council (Grant No. 786707-FunMagResBeacons), and EPSRC-UK (Grant Nos. EP/P009980/1, EP/P030491/1, and EP/V055593/1). We thank Soumya Singha Roy for discussions and Marcel Utz and Andrey Pravdivtsev for comments on the manuscript. We thank Weidong Gong for instrumental help and one of the referees for bringing stimulated nuclear polarization to our attention.[4]

The authors have no conflicts to disclose.

APPENDIX: WOLF PULSE DYNAMICS

The complete Hamiltonian given by Eq. (7) preserves the total z-angular momentum of the following system:

$$[H(t), I_{1z} + I_{2z} + S_{3z}] = 0. \tag{A1}$$

This suggests that the basis states highlighted in Fig. 1 separate the matrix representation of $H(t)$ into two 3×3 and two 1×1 blocks. The 1×1 blocks may be disregarded, and the 3×3 blocks are generated by the following sets:

$$\begin{aligned} V &= \{|S_0\alpha\rangle, |T_0\alpha\rangle, |T_{+1}\beta\rangle\}, \\ W &= \{|S_0\beta\rangle, |T_0\beta\rangle, |T_{-1}\alpha\rangle\}. \end{aligned} \tag{A2}$$

© Author(s) 2021

The standard WEREWOLF experiment (Fig. 4) aims to create positive heteronuclear magnetization, which may be achieved through a population swap of states $|S_0\beta\rangle$ and $|T_{-1}\alpha\rangle$. We thus consider the restriction of $H(t)$ to W, which may be explicitly given as follows:

$$[H(t)]_W = \begin{bmatrix} \frac{1}{2}(B(t)\gamma_S - 3\pi J_{12}) & \frac{\pi}{2}(J_{23} - J_{13}) & \frac{\pi}{\sqrt{2}}(J_{13} - J_{23}) \\ \frac{\pi}{2}(J_{23} - J_{13}) & \frac{1}{2}(B(t)\gamma_S + \pi J_{12}) & \frac{\pi}{\sqrt{2}}(J_{13} + J_{23}) \\ \frac{\pi}{\sqrt{2}}(J_{13} - J_{23}) & \frac{\pi}{\sqrt{2}}(J_{13} + J_{23}) & \left(\gamma_I - \frac{1}{2}\gamma_S\right)B(t) + \frac{\pi}{2}(J_{12} - J_{13} - J_{23}) \end{bmatrix}, \tag{A3}$$

where

$$B(t) = B_{\text{bias}} + B^0_{\text{WOLF}}\cos(\omega_{\text{WOLF}}t). \tag{A4}$$

Although small, the mixing between the states $|S_0\alpha\rangle$ and $|T_0\alpha\rangle$ is not negligible during the WOLF pulse dynamics. To account for the mixing, we define a set of rotated basis states,

$$\begin{aligned} W_\theta &= \{|S'_0\beta\rangle, |T'_0\beta\rangle, |T'_{-1}\alpha\rangle\} \\ &= \{\cos(\theta/2)|S_0\beta\rangle + \sin(\theta/2)|T_0\beta\rangle \times \cos(\theta/2)|T_0\beta\rangle - \sin(\theta/2)|S_0\beta\rangle, |T_{-1}\alpha\rangle\}, \end{aligned} \tag{A5}$$

parameterized by the angle θ. The angle θ is chosen to satisfy

$$\theta = \arctan2(2J_{12}, J_{13} - J_{23}). \tag{A6}$$

In the near-equivalence regime, the matrix representation of $H(t)$ restricted to W_θ is given by

$$[H(t)]_{W_\theta} \simeq \begin{bmatrix} \frac{1}{2}(B(t)\gamma_S - 3\pi J_{12}) & 0 & \frac{\pi}{\sqrt{2}}(\cos(\theta/2)(J_{13} - J_{23}) + \sin(\theta/2)(J_{13} + J_{23})) \\ 0 & \frac{1}{2}(B(t)\gamma_S + \pi J_{12}) & \frac{\pi}{\sqrt{2}}(\cos(\theta/2)(J_{13} + J_{23}) - \sin(\theta/2)(J_{13} - J_{23})) \\ \blacksquare & \blacksquare & \left(\gamma_I - \frac{1}{2}\gamma_S\right)B(t) + \frac{\pi}{2}(J_{12} - J_{13} - J_{23}) \end{bmatrix}, \tag{A7}$$

where the black squares should be replaced by the elements on the opposite side of the diagonal so that the matrix is invariant under transposition.

According to Eq. (A7), the transition frequency between states $|S'_0\beta\rangle$ and $|T'_{-1}\alpha\rangle$ in the near-equivalence regime is given by

$$\begin{aligned} \omega_{ST} &= \langle T'_{-1}\alpha|H_0|T'_{-1}\alpha\rangle - \langle S'_0\beta|H_0|S'_0\beta\rangle \\ &= B_{\text{bias}}(\gamma_I - \gamma_S) + \frac{\pi}{2}(4J_{12} - J_{13} - J_{23}), \end{aligned} \tag{A8}$$

whereas the transition frequency between $|T'_0\beta\rangle$ and $|T'_{-1}\alpha\rangle$ is given by

$$\begin{aligned} \omega_{TT} &= \langle T'_{-1}\alpha|H_0|T'_{-1}\alpha\rangle - \langle S'_0\beta|H_0|S'_0\beta\rangle \\ &= B_{\text{bias}}(\gamma_I - \gamma_S) - \frac{\pi}{2}(J_{13} + J_{23}). \end{aligned} \tag{A9}$$

Application of a WOLF pulse with $\omega_{\text{WOLF}} = \omega_{ST}$ causes a resonant modulation of the energy difference between states $|S'_0\beta\rangle$ and $|T'_{-1}\alpha\rangle$ but causes an off-resonant modulation of the energy difference between states $|T'_0\beta\rangle$ and $|T'_{-1}\alpha\rangle$ on the order of $\sim J_{12}$. To a first approximation, we may neglect the state $|T'_0\beta\rangle$ altogether and consider a fictitious two-level system evolving under the Hamiltonian $h(t)$,

$$\begin{aligned} h(t) &= \begin{bmatrix} \langle S'_0\beta|H(t)|S'_0\beta\rangle & \langle S'_0\beta|H(t)|T'_{-1}\alpha\rangle \\ \langle T'_{-1}\alpha|H(t)|S'_0\beta\rangle & \langle T'_{-1}|H(t)|T'_{-1}\alpha\rangle \end{bmatrix} \\ &= \begin{bmatrix} \frac{1}{2}(B(t)\gamma_S - 3\pi J_{12}) & \frac{\pi}{\sqrt{2}}(\cos(\theta/2)(J_{13} - J_{23}) + \sin(\theta/2)(J_{13} + J_{23})) \\ \frac{\pi}{\sqrt{2}}(\cos(\theta/2)(J_{13} - J_{23}) + \sin(\theta/2)(J_{13} + J_{23})) & \left(\gamma_I - \frac{1}{2}\gamma_S\right)B(t) + \frac{\pi}{2}(J_{12} - J_{13} - J_{23}) \end{bmatrix}. \end{aligned} \tag{A10}$$

© Author(s) 2021

In terms of *normalized* Pauli matrices $(\sigma_j/2)$, the Hamiltonian $h(t)$ may be expressed as follows:

$$h(t) = \omega_0\sigma_0 + \omega_x\sigma_x/2 + \omega_z(t)\sigma_z/2, \tag{A11}$$

with

$$\begin{aligned}\omega_0 &= \frac{1}{2}\gamma_I(B_{\text{bias}} + B^0_{\text{WOLF}}\cos(\omega_{ST}t)) - \frac{\pi}{4}(2J_{12} + J_{13} + J_{23}),\\ \omega_x &= \pi\sqrt{2}(\cos(\theta/2)(J_{13} - J_{23}) + \sin(\theta/2)(J_{13} + J_{23})),\\ \omega_z(t) &= -B^0_{\text{WOLF}}(\gamma_I - \gamma_S)\cos(\omega_{ST}t) - \omega_{ST}.\end{aligned} \tag{A12}$$

The Pauli coefficient ω_x may alternatively be expressed as follows:

$$\begin{aligned}\omega_x &= 2\pi\sqrt{J_{13}^2 + J_{23}^2}\sin(\phi + \theta/2),\\ \phi &= \arctan2(J_{13} + J_{23}, J_{13} - J_{23}),\end{aligned} \tag{A13}$$

where we made use of the following relations:

$$\begin{aligned}\sqrt{J_{13} + J_{23}}\sin(\phi) &= (J_{13} - J_{23})/\sqrt{2},\\ \sqrt{J_{13} + J_{23}}\cos(\phi) &= (J_{13} + J_{23})/\sqrt{2}.\end{aligned} \tag{A14}$$

Within our approximations, the ω_0-term introduces an overall phase shift and may be discarded. The WOLF pulse dynamics may now be approximately described within a "jolting" interaction frame.[10] The jolting frame represents a rotating frame with a time-dependent rotation frequency. The time-dependent rotation frequency and the rotation angle $\psi(t)$ are related as follows:

$$\psi(t) = \int_0^t \omega_z(s)ds. \tag{A15}$$

The jolting frame Hamiltonian $\tilde{h}(t)$ is then given by

$$\begin{aligned}\tilde{h}(t) &= \frac{\omega_x}{2}\exp(+i\psi(t)\sigma_z/2)\sigma_x\exp(-i\psi(t)\sigma_z/2)\\ &= \frac{\omega_x}{4}(\exp(+i\psi(t))\sigma_+ + \exp(-i\psi(t))\sigma_-).\end{aligned} \tag{A16}$$

We may expand the jolting frame Hamiltonian as a Fourier series,

$$\begin{aligned}\tilde{h}(t) = \frac{\omega_x}{4}\Bigg(&\sum_n J_n(A)\exp(-i(n-1)\omega_{ST}t)\sigma_+\\ &+ \sum_n J_{-n}(A)\exp(-i(n+1)\omega_{ST}t)\sigma_-\Bigg),\end{aligned} \tag{A17}$$

where $J_n(x)$ is the nth Bessel function of the first kind and the argument A is defined as follows:

$$A = (\gamma_I - \gamma_S)B^0_{\text{WOLF}}/\omega_{ST}. \tag{A18}$$

For $|\omega_x/\omega_{ST}| \ll 1$, which is bounded from above by

$$|\omega_x/\omega_{ST}| \le 2\pi\sqrt{J_{13}^2 + J_{23}^2}/|\omega_{ST}|, \tag{A19}$$

we may neglect the time-dependent terms of $\tilde{h}(t)$. This approach is equivalent to truncating the average Hamiltonian after first order,[38]

$$\begin{aligned}\tilde{h}(t) &\simeq \frac{\omega_x}{4}(J_1(A)\sigma_+ + J_1(A)\sigma_-)\\ &= \omega_x J_1(A)\sigma_x/2.\end{aligned} \tag{A20}$$

The effective nutation frequency of a WOLF pulse is thus given by

$$\omega^{ST}_{\text{nut}} = \omega_x J_1(A) = 2\pi\sqrt{J_{13}^2 + J_{23}^2}\sin(\phi + \theta/2)J_1(A). \tag{A21}$$

DATA AVAILABILITY

The data that support the findings of this study are available from the corresponding author upon reasonable request.

REFERENCES

[1] R. R. Ernst, G. Bodenhausen, and A. Wokaun, *Principles of Nuclear Magnetic Resonance in One and Two Dimensions* (Clarendon Press, Oxford, 1987).
[2] R. Tycko and S. J. Opella, "Overtone NMR spectroscopy," J. Chem. Phys. **86**, 1761–1774 (1987).
[3] W. T. Wenckebach, "The solid effect," Appl. Magn. Reson. **34**, 227–235 (2008).
[4] R. Z. Sagdeev and E. G. Bagryanskaya, "Stimulated nuclear polarization - a new method for studying the mechanisms of photochemical reactions," Pure Appl. Chem. **62**, 1547–1556 (1990).
[5] J. W. Blanchard, T. F. Sjolander, J. P. King, M. P. Ledbetter, E. H. Levine, V. S. Bajaj, D. Budker, and A. Pines, "Measurement of untruncated nuclear spin interactions via zero- to ultralow-field nuclear magnetic resonance," Phys. Rev. B **92**, 220202 (2015).
[6] R. L. Hesketh and K. M. Brindle, "Magnetic resonance imaging of cancer metabolism with hyperpolarized ^{13}C-labeled cell metabolites," Curr. Opin. Chem. Biol. **45**, 187–194 (2018).
[7] G. Pileio, M. Carravetta, and M. H. Levitt, "Extremely low-frequency spectroscopy in low-field nuclear magnetic resonance," Phys. Rev. Lett. **103**, 083002 (2009).
[8] T. F. Sjolander, M. C. D. Tayler, J. P. King, D. Budker, and A. Pines, "Transition-selective pulses in zero-field nuclear magnetic resonance," J. Phys. Chem. A **120**, 4343–4348 (2016).
[9] M. C. D. Tayler and M. H. Levitt, "Singlet nuclear magnetic resonance of nearly-equivalent spins," Phys. Chem. Chem. Phys. **13**, 5556–5560 (2011).
[10] P. Caravatti, G. Bodenhausen, and R. R. Ernst, "Selective pulse experiments in high-resolution solid state NMR," J. Magn. Reson. **55**, 88–103 (1983).
[11] C. R. Bowers and D. P. Weitekamp, "Transformation of symmetrization order to nuclear-spin magnetization by chemical reaction and nuclear magnetic resonance," Phys. Rev. Lett. **57**, 2645–2648 (1986).
[12] C. R. Bowers and D. P. Weitekamp, "Parahydrogen and synthesis allow dramatically enhanced nuclear alignment," J. Am. Chem. Soc. **109**, 5541–5542 (1987).
[13] R. W. Adams, J. A. Aguilar, K. D. Atkinson, M. J. Cowley, P. I. P. Elliott, S. B. Duckett, G. G. R. Green, I. G. Khazal, J. Lopez-Serrano, and D. C. Williamson, "Reversible interactions with para-hydrogen enhance NMR sensitivity by polarization transfer," Science **323**, 1708–1711 (2009).
[14] B. Ripka, J. Eills, H. Kouřilová, M. Leutzsch, M. H. Levitt, and K. Münnemann, "Hyperpolarized fumarate via parahydrogen," Chem. Commun. **54**, 12246–12249 (2018).
[15] M. Goldman and H. Jóhannesson, "Conversion of a proton pair para order into ^{13}C polarization by rf irradiation, for use in MRI," C. R. Phys. **6**, 575–581 (2005).
[16] S. Kadlecek, K. Emami, M. Ishii, and R. Rizi, "Optimal transfer of spin-order between a singlet nuclear pair and a heteronucleus," J. Magn. Reson. **205**, 9–13 (2010).

© Author(s) 2021

[17]T. Theis, M. Truong, A. M. Coffey, E. Y. Chekmenev, and W. S. Warren, "LIGHT-SABRE enables efficient in-magnet catalytic hyperpolarization," J. Magn. Reson. **248**, 23–26 (2014).
[18]J. Eills, G. Stevanato, C. Bengs, S. Glöggler, S. J. Elliott, J. Alonso-Valdesueiro, G. Pileio, and M. H. Levitt, "Singlet order conversion and parahydrogen-induced hyperpolarization of ^{13}C nuclei in near-equivalent spin systems," J. Magn. Reson. **274**, 163–172 (2017).
[19]C. Bengs, L. Dagys, and M. H. Levitt, "Robust transformation of singlet order into heteronuclear magnetisation over an extended coupling range," J. Magn. Reson. **321**, 106850 (2020).
[20]H. Jóhannesson, O. Axelsson, and M. Karlsson, "Transfer of para-hydrogen spin order into polarization by diabatic field cycling," C. R. Phys. **5**, 315–324 (2004).
[21]A. N. Pravdivtsev, A. V. Yurkovskaya, N. N. Lukzen, K. L. Ivanov, and H.-M. Vieth, "Highly efficient polarization of spin-1/2 insensitive NMR nuclei by adiabatic passage through level anticrossings," J. Phys. Chem. Lett. **5**, 3421–3426 (2014).
[22]T. Theis, M. L. Truong, A. M. Coffey, R. V. Shchepin, K. W. Waddell, F. Shi, B. M. Goodson, W. S. Warren, and E. Y. Chekmenev, "Microtesla SABRE enables 10% nitrogen-15 nuclear spin polarization," J. Am. Chem. Soc. **137**, 1404–1407 (2015).
[23]J. Eills, J. W. Blanchard, T. Wu, C. Bengs, J. Hollenbach, D. Budker, and M. H. Levitt, "Polarization transfer via field sweeping in parahydrogen-enhanced nuclear magnetic resonance," J. Chem. Phys. **150**, 174202 (2019).
[24]J. R. Lindale, S. L. Eriksson, C. P. N. Tanner, Z. Zhou, J. F. P. Colell, G. Zhang, J. Bae, E. Y. Chekmenev, T. Theis, and W. S. Warren, "Unveiling coherently driven hyperpolarization dynamics in signal amplification by reversible exchange," Nat. Commun. **10**, 395 (2019).
[25]C. P. N. Tanner, J. R. Lindale, S. L. Eriksson, Z. Zhou, J. F. P. Colell, T. Theis, and W. S. Warren, "Selective hyperpolarization of heteronuclear singlet states via pulsed microtesla SABRE," J. Chem. Phys. **151**, 044201 (2019).
[26]D. A. Barskiy, S. Knecht, A. V. Yurkovskaya, and K. L. Ivanov, "SABRE: Chemical kinetics and spin dynamics of the formation of hyperpolarization," Prog. Nucl. Magn. Reson. Spectrosc. **114–115**, 33–70 (2019).
[27]J. R. Birchall, M. S. H. Kabir, O. G. Salnikov, N. V. Chukanov, A. Svyatova, K. V. Kovtunov, I. V. Koptyug, J. G. Gelovani, B. M. Goodson, W. Pham, and E. Y. Chekmenev, "Quantifying the effects of quadrupolar sinks via ^{15}N relaxation dynamics in metronidazoles hyperpolarized via SABRE-SHEATH," Chem. Commun. **56**, 9098–9101 (2020).
[28]S. Knecht, J. W. Blanchard, D. Barskiy, E. Cavallari, L. Dagys, E. Van Dyke, M. Tsukanov, B. Bliemel, K. Münnemann, S. Aime, F. Reineri, M. H. Levitt, G. Buntkowsky, A. Pines, P. Blümler, D. Budker, and J. Eills, "Rapid hyperpolarization and purification of the metabolite fumarate in aqueous solution," Proc. Natl. Acad. Sci. U. S. A. **118**, e2025383118 (2021).
[29]S. L. Eriksson, J. R. Lindale, X. Li, and W. S. Warren, "Improving SABRE hyperpolarization with highly non-intuitive pulse sequences: Moving beyond avoided crossings to describe dynamics," arXiv:2107.04687 [physics] (2021).
[30]S. J. DeVience, M. Greer, S. Mandal, and M. S. Rosen, "Homonuclear J coupling spectroscopy at low magnetic fields using spin-lock induced crossing," Chem. Phys. Chem. (2021).
[31]L. Wienands, F. Theiß, J. Eills, L. Rösler, S. Knecht, and G. Buntkowsky, "Optimizing the reaction conditions for the formation of fumarate via trans-hydrogenation," Appl. Magn. Reson. 1–20 (2021).
[32]C. Bengs and M. H. Levitt, "SpinDynamica: Symbolic and numerical magnetic resonance in a mathematica environment," Magn. Reson. Chem. **56**, 374–414 (2018).
[33]B. A. Rodin, J. Eills, R. Picazo-Frutos, K. F. Sheberstov, D. Budker, and K. L. Ivanov, "Constant-adiabaticity ultralow magnetic field manipulations of parahydrogen-induced polarization: Application to an AA'X spin system," Phys. Chem. Chem. Phys. **23**, 7125–7134 (2021).
[34]B. A. Rodin, V. P. Kozinenko, A. S. Kiryutin, A. V. Yurkovskaya, J. Eills, and K. L. Ivanov, "Constant-adiabaticity pulse schemes for manipulating singlet order in 3-spin systems with weak magnetic non-equivalence," J. Magn. Reson. **327**, 106978 (2021).
[35]S. Knecht, A. S. Kiryutin, A. V. Yurkovskaya, and K. L. Ivanov, "Mechanism of spontaneous polarization transfer in high-field SABRE experiments," J. Magn. Reson. **287**, 74–81 (2018).
[36]S. Knecht, S. Hadjiali, D. A. Barskiy, A. Pines, G. Sauer, A. S. Kiryutin, K. L. Ivanov, A. V. Yurkovskaya, and G. Buntkowsky, "Indirect detection of short-lived hydride intermediates of iridium N-heterocyclic carbene complexes via chemical exchange saturation transfer spectroscopy," J. Phys. Chem. C **123**, 16288–16293 (2019).
[37]M. H. Levitt, "Composite pulses," Prog. Nucl. Magn. Reson. Spectrosc. **18**, 61–122 (1986).
[38]U. Haeberlen and J. S. Waugh, "Coherent averaging effects in magnetic resonance," Phys. Rev. **175**, 453 (1968).

© Author(s) 2021